THE EFFECT OF COMBUSTION CHAMBER GEOMETRY LAYOUT ON COMBUSTION AND EMISSION

by

Zoran S. JOVANOVIĆ, Stojan V. PETROVIĆ, and Miroljub V. TOMIĆ

Original scientific paper
UDC: 662.767:66.011
BIBLID: 0354-9836, *12* (2008), 1, 7-24
DOI: 10.2298/TSCI0801007J

In this paper some results concerning the combined effect of the tumble flow and combustion chamber geometry layout variations on flame front shape and its propagation through homogenous mixture of isooctane and air are presented. Spatial distributions of NO in different combustion chamber geometries are presented as well. The basic combustion chamber geometry layout considered consists of the flat head with two vertical valves and a cylindrical bowl subjected to variations of depth and squish area. All results presented were obtained by dint of multidimensional modeling of reactive flows in arbitrary geometry with moving objects and boundaries with modified KIVA3 and KIVA3V source codes. Two additional computer codes were applied to generate boundary conditions for KIVA3V calculations with moving valves. The AVL TYCON code was used for the calculation of valve lift profiles, and AVL BOOST code was used for the calculation of relevant data set in the valve regions. Different combustion chamber geometry layouts generate different levels of squish, and the combustion effects in essence depend on the interaction of that flow with tumble. It was found that for particular combustion chamber shapes with different diameter/depth aspect ratios entirely different flame front shapes and propagation velocities were encountered primarily due to variations of fluid flow patterns in the vicinity of top dead center.

Key words: *combustion, 3-D fluid flow, flame propagation*

Introductory remarks

It is known for a long time that various types of organized flows in combustion chamber of spark ignition (SI) engines are of critical importance for combustion, particularly with regards to flame front shape and its propagation [1, 2]. Some results related to synergic effect of squish and swirl on flame front shape and its propagation through various combustion chamber layouts were already analyzed in previously published papers [3, 9-12, 18]. However, the isolated or combined effect of the third type of organized flow *i. e.* the effect of tumble or "tumble-like" intake flow on flame front shape and its displacement is not sufficiently clarified ensuing in part due to the ambiguity concerning the exact definition of tumble flow. Namely, in spite of the fact that tumble flow is inherent to multi-valve engines some two valve engines exhibit characteristics similar to tumble flow [4, 8, 13-17]. In the rest of the paper, in lieu of tumble or tumble-like flow we are considering a more general intake flow. In addition, one of the reason is also computational fluid dynamics (CFD) with all the difficulties ensuing from 3-D grid generation of real multi-cylinder engine and experimental verification of numerical results. For that reason, in this paper, the com-

bined effect of squish and intake flow on flame front shape and its propagation was analyzed as a part of a broader, more general, research concerning the effect of intake port/valve geometry and combustion chamber layout variations on flame parameters. One of the goals was to establish if the full control of flame front shape and its propagation can be achieved through squish variation only. For that reason numerical results of flame front shape and its propagation, for the case with no intake flow (no valves), were presented in chapter *The isolated effect of squish*, and compared with numerical results of flame front shape and its propagation, for the case with valves, presented in chapter *The combined effect of squish and intake flow*.

Combustion modeling

The analysis of this type requires multidimensional numerical modeling of reactive flows in complicated geometry. Therefore a KIVA3V code [5] was applied for the analysis of the effect of intake flow modeling on flame parameters. The code encompasses the valve/port geometry in an explicit manner. Taking into account various options contained in aforementioned code the following assumptions were adopted:

- flame propagation is controlled by turbulent diffusion modeled via a k-ε model of turbulence,
- chemistry was modeled with quasi global irreversible reaction of iso octane oxidation (C_8H_{18}) followed by two group of reactions, those which proceed kinetically and those which reduce the chemical heat release,
- the ignition was not modeled but rather by-passed and replaced by-energy deposition in spark cells (artificial rise of temperature in spark cells),
- the commencement and the length of energy deposition was not adjusted with reference to the location of peak cylinder pressure determined with BOOST code [7],
- in the case with valves the relevant set of data on open boundaries were calculated with BOOST code as well, and
- valve lift curves and valve timing were calculated through series calculations with TYCON code [6].

Results

The isolated effect of squish

The analysis of the isolated effect of squish on fluid flow pattern, flame front shape and its propagation were obtained through squish area variation (SA) from 23 to 63%, as related to bore cross-section. The combustion chamber geometry layouts are shown in a form of axonometric plots in figs. 1-3.

It can be seen that combustion chamber is in form of cylindrical bowl with variable diameter and depth ranging from 2.533, 2.806, 3.071, 3.34, and 3.609 cm to 1.383, 1.155, 0.9653, 0.815, and 0.698 cm, respectively. The compression ratio was kept at 9.5. Supplementary data to be taken into account are bore/stroke ratio = 8.25/9.2, total cylinder displacement = 550 cm^3, volumetric efficiency η = 0.82, mixture quality λ = 1, and engine speed n = 2000 per minute. The fluid flow pattern during compression, for all five cases, is mainly controlled by piston motion and is similar except in the vicinity of top dead center (TDC). The flow field pattern represented as velocity vectors in x-z plane for the case with SA = 23% is shown in fig. 4.

It can be seen that due to ingress of fluid from squish zone small vortices in clockwise direction with regard to the left side, provided that it is stipulated as such, are formed around the per-

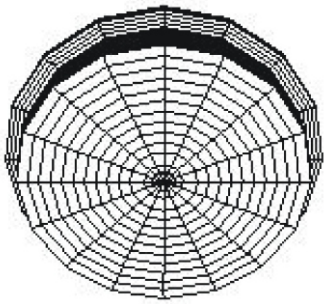

Figure 1. Axonometric plot of combustion chamber with SA = 23% (no valves)

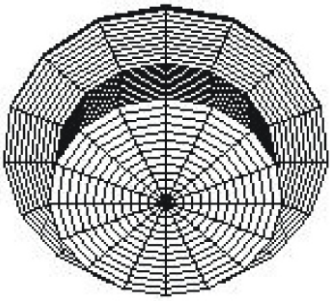

Figure 2. Axonometric plot of combustion chamber with SA = 54% (no valves)

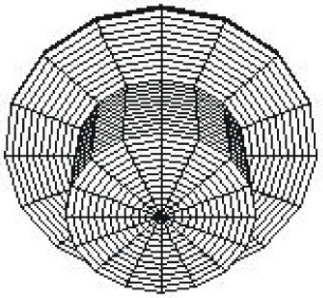

Figure 3. Axonometric plot of combustion chamber with SA = 63% (no valves)

imeter of cylindrical bowl (see fig. 4). Under the influence of flame arrival (larger velocities in front of the flame front) these vortices are reducing their size and the entire flow field is is generally flame dominated (see fig. 7). The fairly similar situation is obtained for SA = 34%. On the contrary the situation is slightly different for case with SA = 44 and SA = 54% (shown in fig. 5).

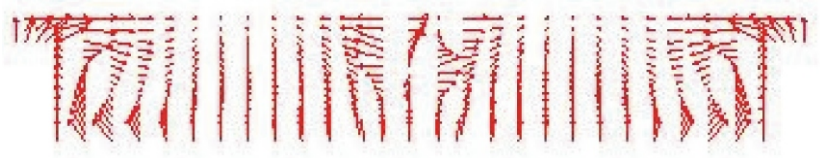

Figure 4. Flow field pattern in x-z plane, y = 0, at –9.78 deg aTDC (SA = 23%, no valves, extreme case) (color image see on our web site)

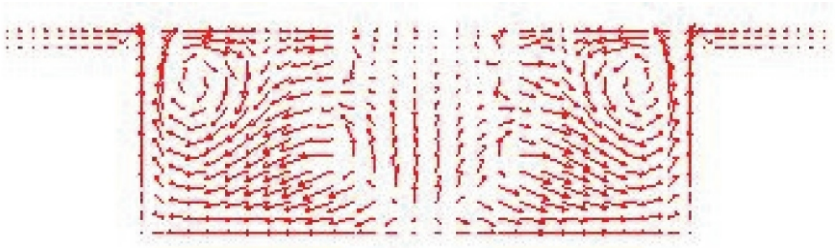

Figure 5. Flow field pattern in x-z plane, y = 0, at –0.01 deg aTDC (SA = 54%, no valves, real case) (color image see on our web site)

No quiescent zone exists anywhere except in the soothing zone behind the flame front. Vortex flow around the perimeter of the bowl is well formed and strong enough to reach the zone in front of the flame front but not to the extent to deteriorate it. Obviously, thyroidal vortex, located around the perimeter of the bowl, rotates in the direction, inward, to the central part of the chamber, encounters fluid flow in front of the flame front, merges with it and contributes to the overall acceleration of the fluid flow in that region. The net result of coinciding flow observed in that region is flame acceleration in that region as well.

In the case with SA = 63% (fig. 6) the flow field and the flame propagation are entirely squish dominated instead of flame dominated as it was the case with SA in the range from 23 to 44%. The vortex flow around the perimeter of the bowl is excessively strong and protrudes inwards to the extent that it constrains the flame propagation particularly in the upper part of the combustion chamber. It is interesting to note that in the case of flame dominated flows the maximum kinetic energy of turbulence is located in the central part of the chamber indicating that the effect of squish flow is negligible.

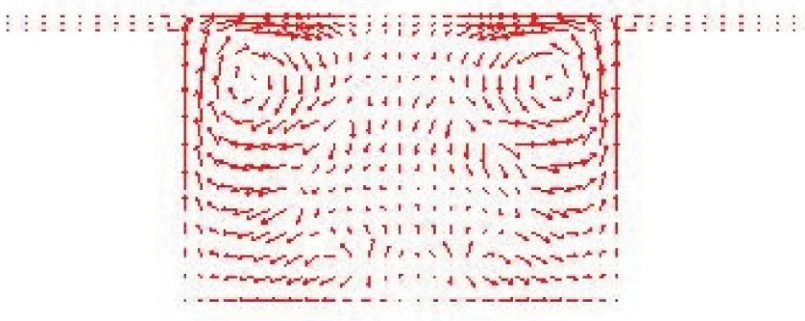

Figure 6. Flow field pattern in x-z plane, y = 0, at 0.06 deg aTDC (SA = 63%, no valves, extreme case) (color image see on our web site)

The flame propagation through combustion chamber considered is represented in form of iso contours of temperatures ranging from minimum to maximum and is shown for corresponding SA cases in figs. 7-9. The exact location of the flame front is determined in the zone of maximum line densities due to equal temperature difference of iso contours. Spark plug is located on z-axis in all five cases. Flame propagation through unburned mixture is controlled, excluding macro flows, by turbulent diffusion *i. e*. by high intensity of turbulence and cascade pro-

Figure 7. Spatial distribution of iso contours of temperature in x-z plane, y = 0, at 0.06 deg aTDC (SA = 23%, no valves, extreme case) (color image see on our web site)

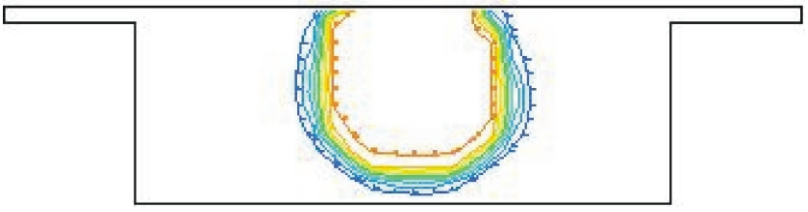

Figure 8. Spatial distribution of iso contours of temperature in x-z plane, y = 0, at 0.06 deg aTDC (SA = 54%, real case) (color image see on our web site)

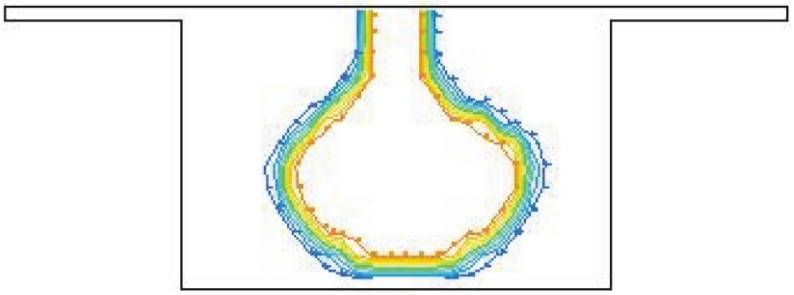

Figure 9. Spatial distribution of iso contours of temperature in x-z plane, y = 0, at 0.06 deg aTDC (SA = 63%, no valves, extreme case) (color image see on our web site)

cess of tearing or breaking up large vortices into smaller ones fully complying with assumptions imposed by k-ε model of turbulence. Anyhow, at least five conflicting mechanisms, acting in concert, described in [1, 2] are of prime importance for the determination of flame front shape and its displacement. These are, *inter alia*, flame generated turbulence, compression by the flame, increase of the viscosity behind the flame front, the sign and the magnitude of the density gradient across the flame front, and the effect of large heat release due to chemical reactions.

As can be seen in fig. 7 for the case with insufficient squish effect (flame dominated flows) the flame front shape is widen, its propagation slow and controlled solely by aforementioned mechanisms. For the case with SA = 54%, shown in fig. 8, the full support of macro flows is encountered.

The flame front shape is nearly spherical and it propagates faster than in previous cases. The larger velocities in front of the flame front coincide with vortex flow around the perimeter of the bowl causing faster flame propagation thereafter.

Finally, for the case with SA = 63%, shown in fig. 9, all negative aspects concerning squish dominated flame are clearly legible. Namely, we are nearly faced with the break up of the flame front in the upper part of the chamber. In addition, the tip of the flame front, being expelled downward, along the z-axis, forms the mushroom shape yielding the appearance of pockets of unburned mixture in the upper part of the combustion chamber in the later phase.

The combined effect of squish and itake flow

The analysis of the combined effect of squish and intake flow on flame front shape and its displacement was carried out for identical combustion chamber geometry layouts as in section *The isolated effect of squish, i. e.* for SA in the range from 23 to 63%, shown in figs. 10-12.

According to the results, presented in section *The isolated effect of squish*, it was quite obvious that two insufficient squish cases (flame dominated flows) were entirely irrelevant (SA = = 23%, SA = 34%) and therefore excluded from the analysis. In these two cases flame propagation behaves as in the case with flat piston.

In the case with valves, combustion chambers, shown in figs. 10-12, were treated as an integral part of the complete engine shown in fig. 13.

As can be seen in fig. 13, in addition to the single cylinder (C1), various components such as air cleaner (F1), plenum chambers (P11, P12, P13), bending (5), restrictions (R1-R3), and pipes of definite lengths and diameters are included (1-11). The distance of two reference points (MP5 and MP6) were specified in such a way to correspond to the location of open

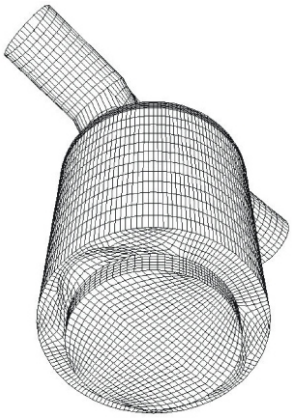

Figure 10. Axonometric plot of the cylindrical combustion chamber (SA = 44%) with valves

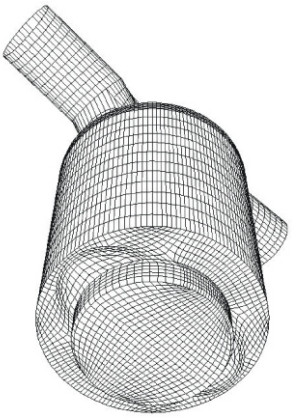

Figure 11. Axonometric plot of the cylindrical combustion chamber (SA = 54%) with valves

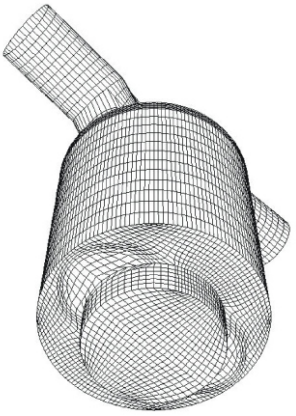

Figure 12. Axonometric plot of the cylindrical combustion chamber (SA = 63%) with valves

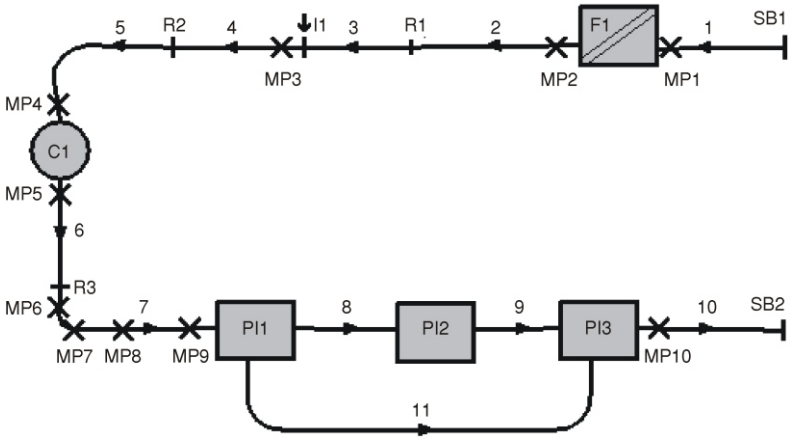

Figure 13. Schematic presentation of the complete engine

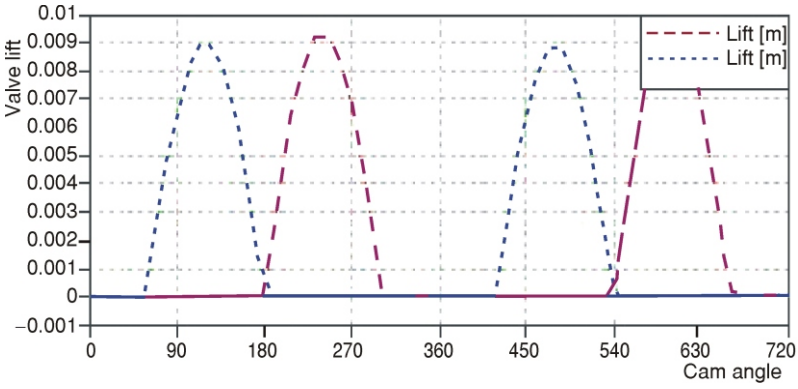

Figure 14. Calculated valve lift curves *vs.* cam angle (color image see on our web site)

boundaries (SB1, SB2) in figs. 10-12. Each element requires pertinent set of specifications. Namely, for a cylinder it implies, in addition to the valve/port specifications (port surface areas,

port wall temperature, geometry of valve assembly, clearance, valve lift curves, valve timings, *etc*.) the geometry of the chamber (Heron, no offset, as shown in figs. 10-12), spark plug location, ignition timing, *etc*. The valve lift curves for the single cylinder, shown in fig. 14, were calculated with TYCON code [6], spread out along crank angle, appropriately shifted and included in both BOOST [7] and KIVA3V [5] codes.

For the purpose of ignition and valve timing optimizations and in order to obtain the appropriate set of requisite values for KIVA3V code such as pressures (fig. 15), temperatures (fig. 16), velocities, species densities, and turbulence parameters, a large number of preliminary engine cycle calculations (transients, traces, series) were carried out with BOOST code.

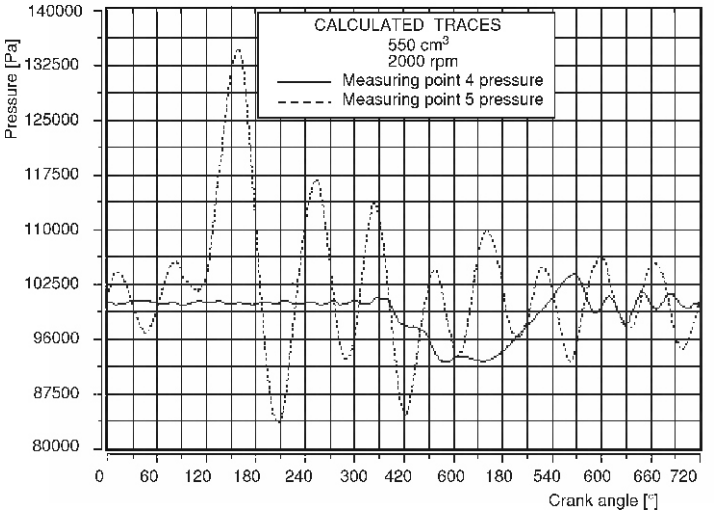

Figure 15. Pressure *vs.* crank angle at reference points MP5 and MP6 for SA = 54%

The slightly different values obtained for different SA were appropriately included in KIVA3V code.

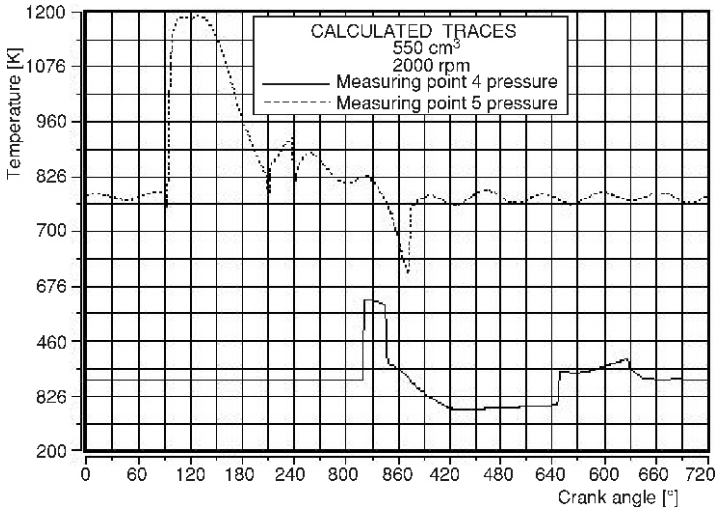

Figure 16. Temperature *vs.* crank angle at reference points MP5 and MP6 for SA = 54%

The evolution of the fluid flow pattern for combustion chamber geometry layouts with valves is shown in figs. 17-22.

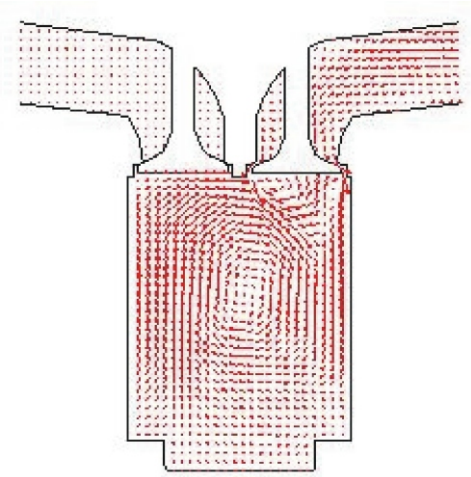

Figure 17. Fluid flow pattern in x-z plane, y = 0, at 180 deg aTDC (SA = 54%) (color image see on our web site)

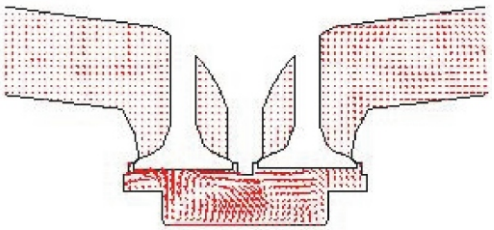

Figure 19. Fluid flow pattern in x-z plane, y = 0, at 350 deg aTDC (SA = 54%) (color image see on our web site)

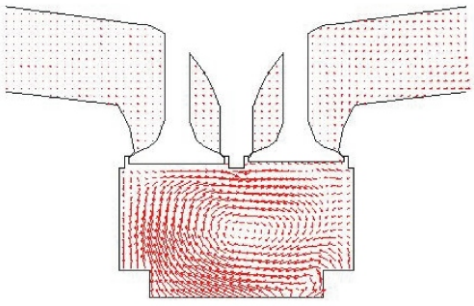

Figure 21. Fluid flow pattern in x-z plane, y = 0, at 300 deg aTDC (SA = 44%) (color image see on our web site)

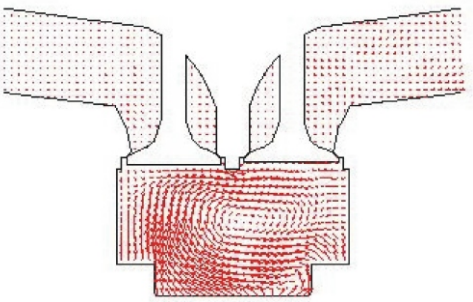

Figure 18. Fluid flow pattern in x-z plane, y = 0, at 300 deg aTDC (SA = 54%) (color image see on our web site)

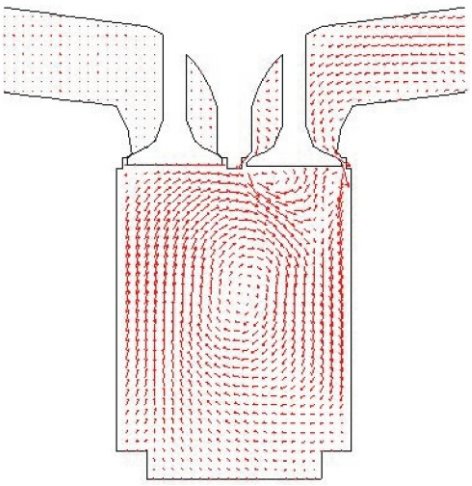

Figure 20. Fluid flow pattern in x-z plane, y = 0, at 180 deg aTDC (SA = 44%) (color image see on our web site)

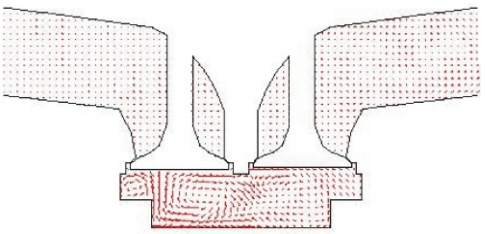

Figure 22. Fluid flow pattern in x-z plane, y = 0, at 350 deg aTDC (SA = 44%) (color image see on our web site)

During opening of intake valve the intake flow hits the piston crown, curls and commences to form the vortex flow around y-axis with its center of rotation in the zone beneath the exhaust valve. At the same time the intake flow strikes upon the cylinder wall, rebounds, hits the piston crown, curls and hits the face of intake valve promoting the fluid flow separation and forming of two vortices, the first one located beneath the left side of intake valve face coinciding with vortex flow around y-axis and the second located beneath the right side of intake valve face rotating in the opposite direction. During induction the intensity of vortex flow around y-axis is increasing and its center of rotation gradually shifting to the central part of combustion chamber. In addition, the vortex flow due to separation, being squeezed by vortex flow around y-axis reaches the narrow zone in the close proximity of intake valve affecting that zone only while the other vortex flow due to separation is pushed to the cylinder wall (figs. 17, 20). Obviously, in the case with valves the fluid flow pattern at the very beginning of compression is entirely different in comparison with zero velocity field. The higher intensity of vortex flow around y-axis during compression promotes the destruction of all vortex flows, except those around z-axis and at 300 deg aTDC its center of rotation is entirely displaced in the zone beneath the intake valve. At that angle commences the stretching of the vortex flow around y-axis *i. e*. the vortex flow around y-axis is subjected to compression by piston movement and slowly squeezed out from the intake valve zone (figs. 18, 21). The squeezing out of vortex flow around y-axis continues up to 350 deg aTDC when there is no vortex flow in the intake valve zone. On the contrary, in the exhaust valve zone the vortex flow around y-axis exhibits the certain effect (figs. 19, 22). Namely, in the case with valves during induction and compression the center of rotation of vortex flow around y-axis is gradually displaced from exhaust valve zone to intake valve zone and *vice versa*. The existence of vortex flow around y-axis in the exhaust valve zone in the vicinity of TDC dominantly affects the flame front shape and its propagation. In the case with no valves such a vortex flow was not encountered. Obviously, fluid flow patterns for SA = 44% and SA = 54% are entirely identical.

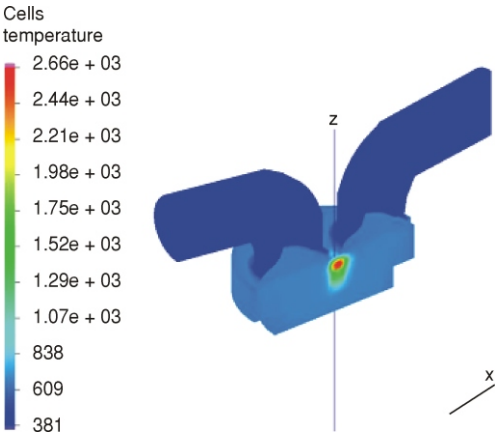

Figure 23. Spatial distribution of iso contours of temperatures at 330 deg aTDC (SA = 44%), perspective plot (azimuth –130°, elevation +30°, twist 0°) (color image see on our web site)

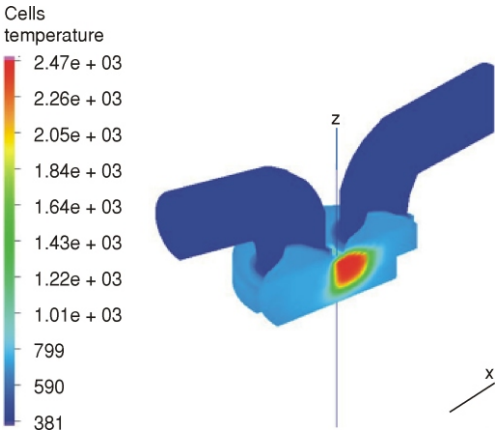

Figure 24. Spatial distribution of iso contours of temperatures at 340 deg aTDC (SA = 44%), perspective plot (azimuth –130°, elevation +30°, twist 0°) (color image see on our web site)

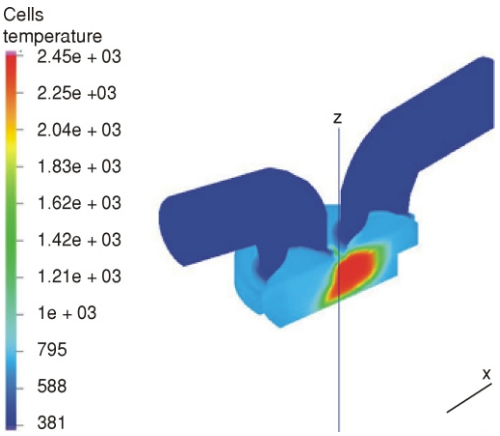

Figure 25. Spatial distribution of isocontours of temperatures at 345 deg aTDC (SA = 44%), perspective plot (azimuth –130°, elevation +30°, twist 0°) (color image see on our web site)

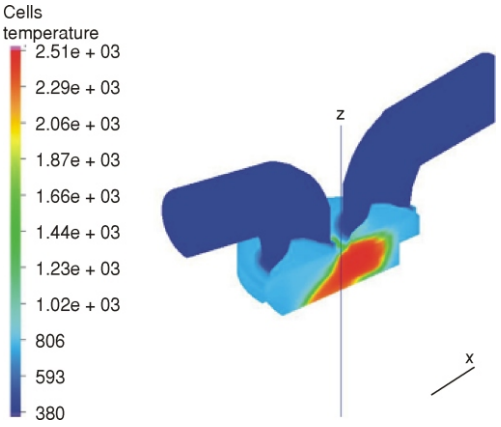

Figure 26. Spatial distribution of isocontours of temperatures at 350 deg aTDC (SA = 44%), perspective plot (azimuth –130°, elevation +30°, twist 0°) (color image see on our web site)

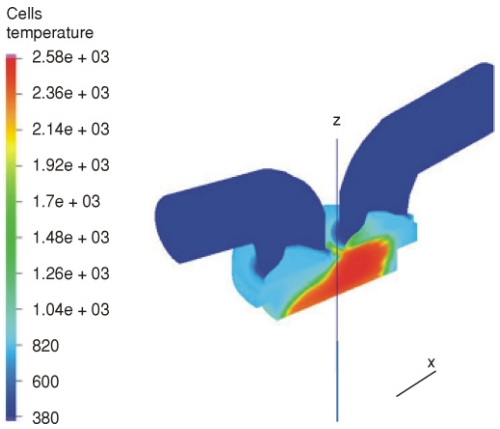

Figure 27. Spatial distribution of isocontours of temperatures at 355 deg aTDC (SA = 44%), perspective plot (azimuth –130°, elevation +30°, twist 0°) (color image see on our web site)

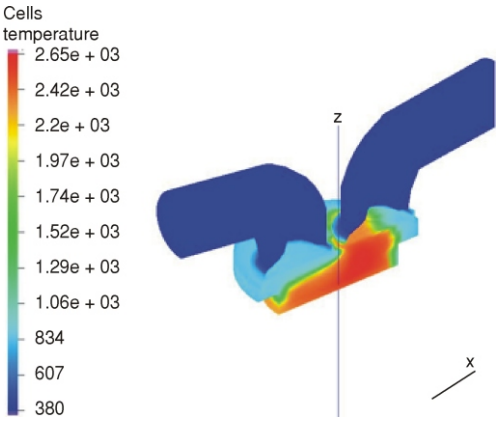

Figure 28. Spatial distribution of isocontours of temperatures at 360 deg aTDC (SA = 44%), perspective plot (azimuth –130°, elevation +30°, twist 0°) (color image see on our web site)

In the case with valves flame front shape and its propagation for squish area of 44% and appropriate angles is shown in figs. 23-29.

Instead of Common Graphycs System [19] used for visualization of all previous results GMV UNIX code [20] was used for the visualization of flame results in the case with valves.

A particularly interesting set of visualizations could emerge, such as those presented in figs. 30 and 31, by dint of adequate combination of azimuth, elevation and twist angles.

These plots were used for the determination of flame propagation velocities thereafter.

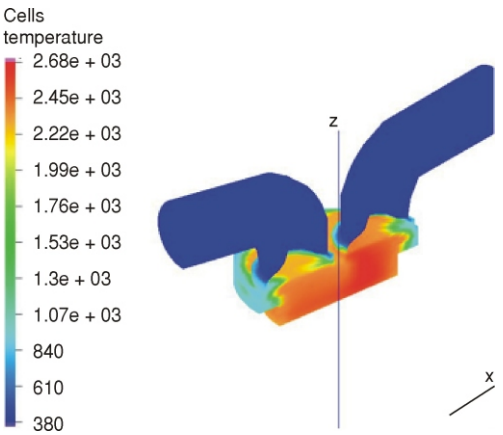

Figure 29. Spatial distribution of isocontours of temperatures at 369 deg aTDC (SA = 44%), perspective plot (azimuth –130°, elevation +30°, twist 0°) (color image see on our web site)

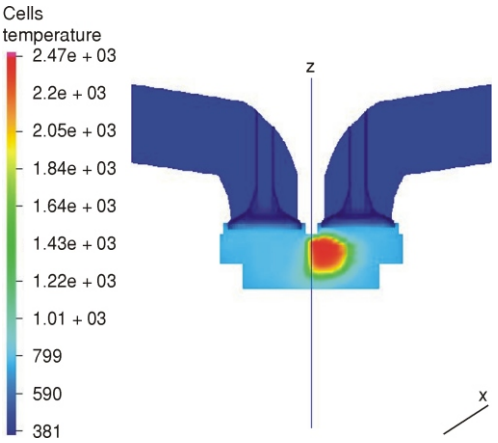

Figure 30. Spatial distribution of isocontours of temperatures in x-z plane, y = 0, at 340 deg aTDC (SA = 44%)(azimuth –90°, elevation 0°, twist 0°) (color image see on our web site)

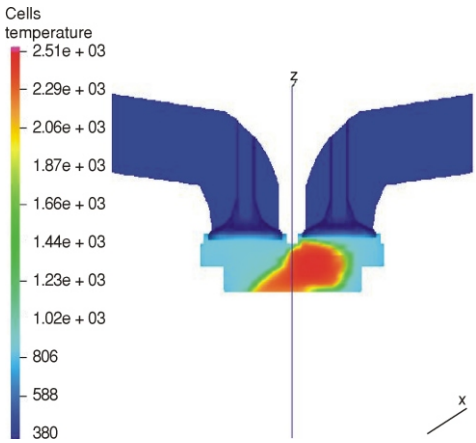

Figure 31. Spatial distribution of isocontours of temperatures in x-z plane, y = 0, at 360 deg aTDC (SA = 44%) (azimuth –90°, elevation 0°, twist 0°) (color image see on our web site)

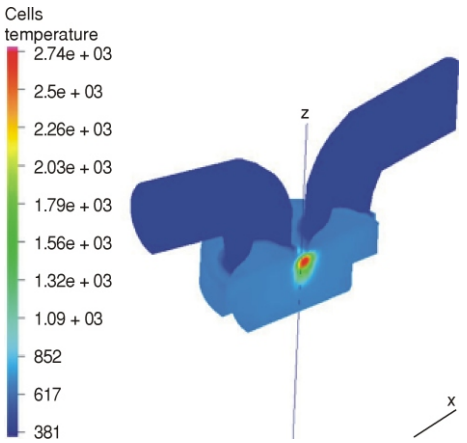

Figure 32. Spatial distribution of isocontours of temperatures at 330 deg aTDC (SA = 54%), perspective plot (azimuth –130°, elevation +30°, twist 0°) (color image see on our web site)

Axonometric plots of flame front shape and its propagation for squish area of 54% and appropriate set of angles, as in the case of SA = 44%, are shown in figs. 32-38.

The appropriate set of plots for determination of flame propagation velocities in the case with SA = 54% are laid down in figs. 39 and 40.

Useful information regarding the flame front shape and its displacement are gained by dint of visualization of isocontours of temperatures in x-y cut planes at different but fixed z-coordinate as shown in figs. 41-48. Only a few selected plots are presented.

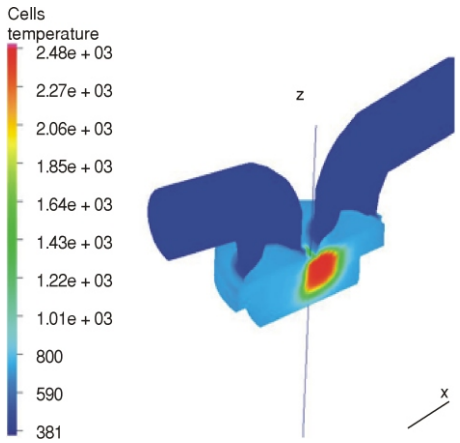

Figure 33. Spatial distribution of isocontours of temperatures at 340 deg aTDC (SA = 54%), perspective plot (azimuth –130°, elevation +30°, twist 0°) (color image see on our web site)

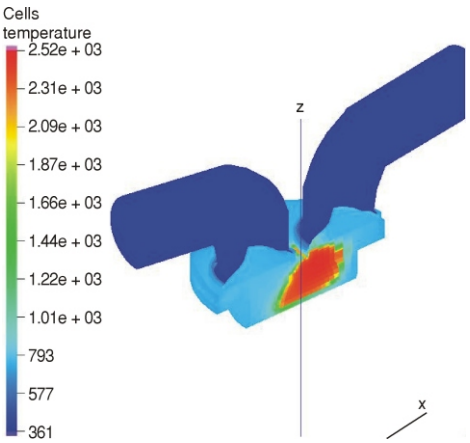

Figure 34. Spatial distribution of isocontours of temperatures at 345 deg aTDC (SA = 54%), perspective plot (azimuth –130°, elevation +30°, twist 0°) (color image see on our web site)

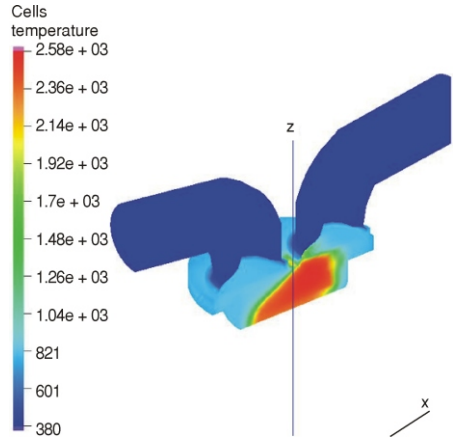

Figure 35. Spatial distribution of isocontours of temperatures at 350 deg aTDC (SA = 54%), perspective plot (azimuth –130°, elevation +30°, twist 0°) (color image see on our web site)

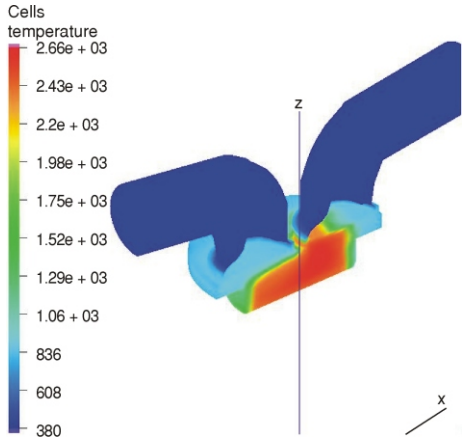

Figure 36. Spatial distribution of isocontours of temperatures at 355 deg aTDC (SA = 54%), perspective plot (azimuth –130°, elevation +30°, twist 0°) (color image see on our web site)

Corresponding plots as regards flame front shape and its displacement in x-z plain (z = = const) for SA = 54% are set forth in figs. 44-47.

As can be seen in figs. 23 and 32 the spark plug is centrally located. Obviously, the flame front shape is extremely irregular and characterized with non uniform spatial propagation for both cases (SA = 44% and SA = 54%). Deflection of the flame commences from the very beginning (time of ignition) and is affected directly by vortex motion around y-axis in the zone beneath exhaust valve. Namely the persistence of vortex flow in the zone beneath exhaust valve is the prime reason for the continuous deflection of the flame front. This deflection is getting more

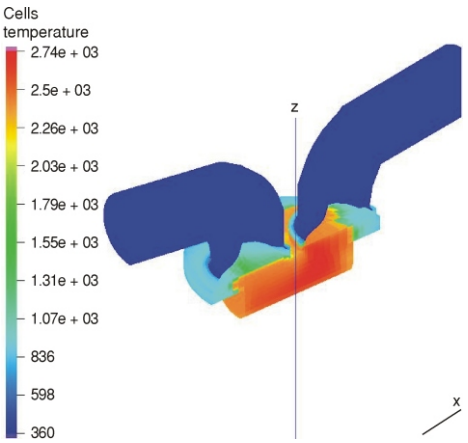

Figure 37. Spatial distribution of isocontours of temperatures at 360 deg aTDC (SA = 54%), perspective plot (azimuth –130°, elevation +30°, twist 0°) (color image see on our web site)

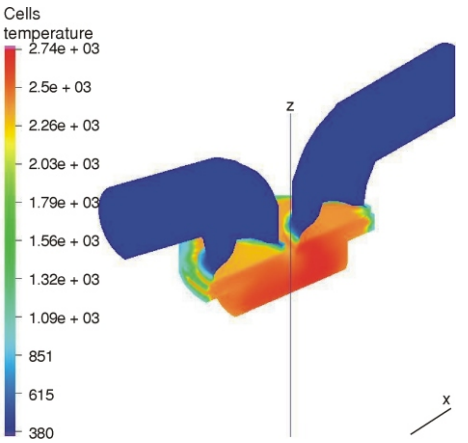

Figure 38. Spatial distribution of isocontours of temperatures at 369 deg aTDC (SA = 54%), perspective plot (azimuth –130°, elevation +30°, twist 0°) (color image see on our web site)

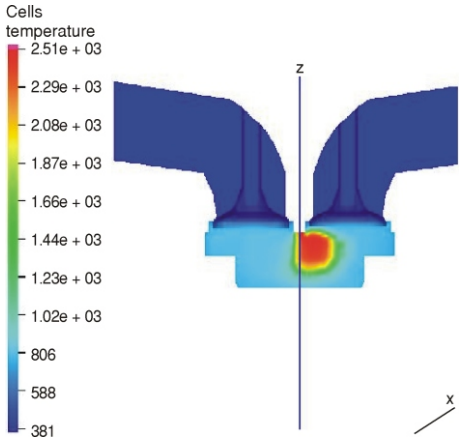

Figure 39. Spatial distribution of isocontours of temperatures in x-z plane, y = 0, at 340 deg aTDS (SA = 54%) (azimuth –90°, elevation 0°, twist 0°) (color image see on our web site)

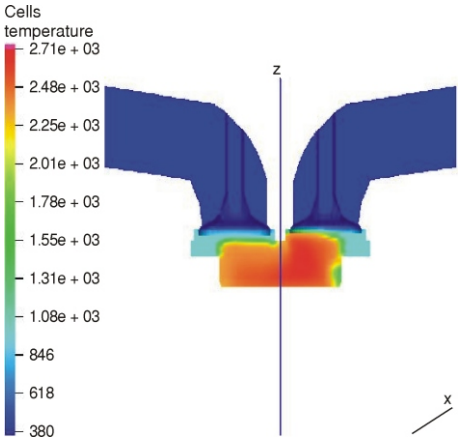

Figure 40. Spatial distribution of isocontours of temperatures in x-z plane, y = 0, at 360 deg aTDC (SA = 54%) (azimuth –90°, elevation 0°, twist 0°) (color image see on our web site)

expressive due to piston movement to TDC and that is fairly legible in plots regarding flame front shape at consecutive angles. Such a trend continues ahead for squish area of SA = 44% (figs. 23-31) and squish area of SA = 54% (figs. 32-40) and yields the appearance of detention zone beneath exhaust valve. Slightly higher kinetic energy of turbulence in the case of SA = = 54% (fig. 50) than in the case with SA = 44% (fig. 49) generates slightly faster flame propagation. In principle, it should be noted that fairly similar situation is encountered for the whole range of squish area (SA = 44% up to SA = 63%) indicating that the effect of squish in the case of intake flow is relatively negligible. Namely, the effect of tumble flow or tumble-like flow

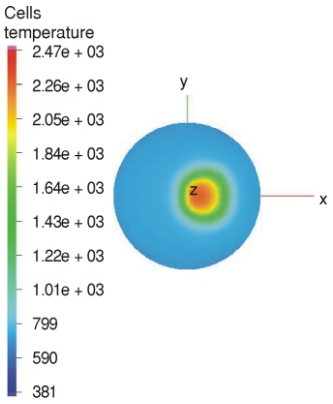

Figure 41. Spatial distribution of isocontours of temperatures in x-y plane, z = 9 cm, at 340 deg aTDC (SA = 44%) (in bowl) (color image see on our web site)

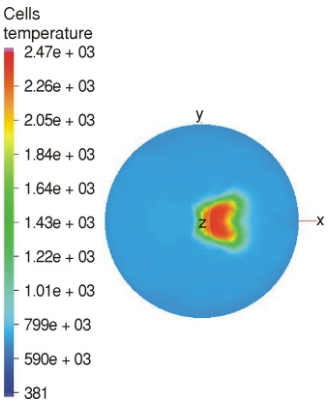

Figure 42. Spatial distribution of isocontours of temperatures in x-y plane, z = 10.2 cm, at 340 deg aTDC (SA = 44%) (color image see on our web site)

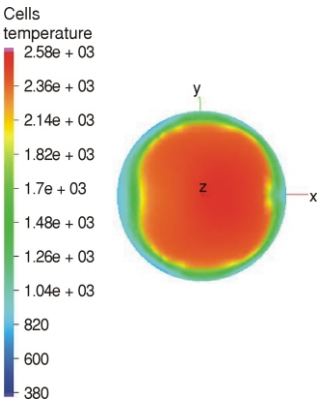

Figure 43. Spatial distribution of isocontours of temperatures in x-y plane, z = 9 cm, at 355 deg aTDC (SA = 44%) (in bowl) (color image see on our web site)

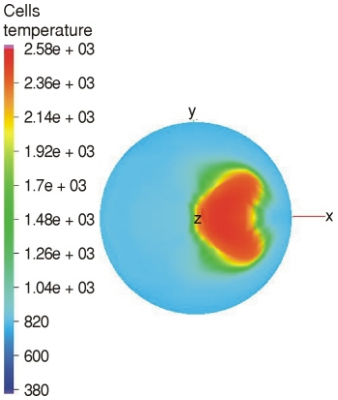

Figure 44. Spatial distribution of isocontours of temperatures in x-y plane, z = 10.2 cm, at 355 deg aTDC (SA = 44%) (color image see on our web site)

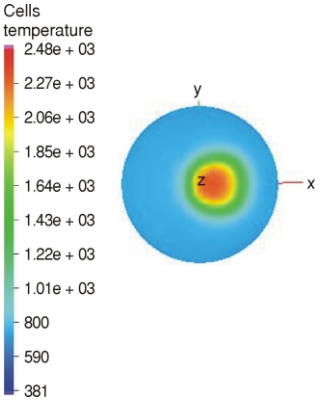

Figure 45. Spatial distribution of isocontours of temperatures in x-y plane, z = 9 cm, at 340 deg aTDC (SA = 54%) (in bowl) (color image see on our web site)

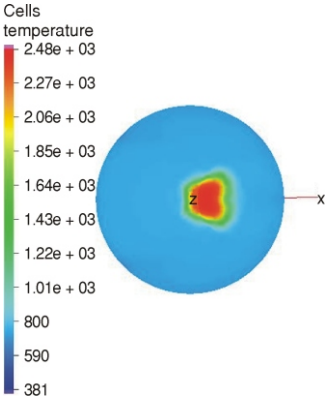

Figure 46. Spatial distribution of isocontours of temperatures in x-y plane, z = 10.2cm, at 340 deg aTDC (SA = 54%) (color image see on our web site)

around y-axis is dominant. The same conclusion can be drawn out from flame front shapes and propagation in x-y cut planes for different crank angle. Namely, the flame front shapes are entirely identical in x-y plane at z = 9 cm (bowl) for the whole range of SA up to 355 deg aTDC as can be seen in figs. 41-47. Slightly larger red and green areas in x-y plane at z = 10.2 cm, in the case with SA = 54% (fig. 48) in comparison with SA = 44% (fig. 44) are due to slightly higher kinetic energy of turbulence (figs. 51 and 52) ensuing from slightly higher vortex intensity in the zone beneath exhaust valve for SA = 54%.

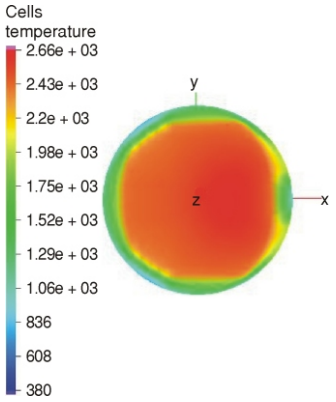

Figure 47. Spatial distribution of isocontours of temperatures in x-y plane, z = 9 cm, at 355 deg aTDC (SA = 54%) (color image see on our web site)

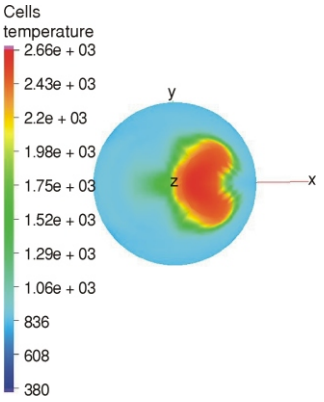

Figure 48. Spatial distribution of isocontours of temperatures in x-y plane, z = 10.2 cm, at 355 deg aTDC (SA = 54%) (color image see on our web site)

The chemistry was represented with one irreversible fuel oxidation reaction (octane) pursued with three slow reactions which proceed kinetically (extended Zeldowich mechanism for NO formation) and six fast reactions which are assumed to be in equilibrium [1, 2, 17]. Twelve components were tackled to in total and their spatial and time distributions, together with other relevant parameters, calculated for different geometry layouts. It should be noted that the number of species and chemical reactions that can be accounted for is arbitrary and is limited only by computer time and storage considerations. Only a few representative results as regards nitric oxide (NO) were selected for presentation in this paper. NO is a high enthalpy component that appears due to high long lasting temperature during combustion. The formation proceeds in the zone of burnt mixture immediately after flame arrival. The certain effect could be imparted to equilibrium concentrations of N, N_2, O_2, O, OH, and H as reactions of NO formation are very slow in comparison to other reactions. The final concentration of NO in any point is affected by the tem-

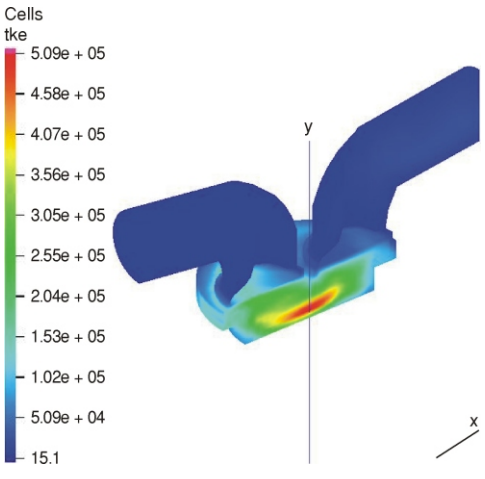

Figure 49. Spatial distribution of isocontours of kinetic energy of turbulence (tke) at 360 deg aTDC (SA = 44%), perspective plot (azimuth –130°, elevation +30°, twist 0°) (color image see on our web site)

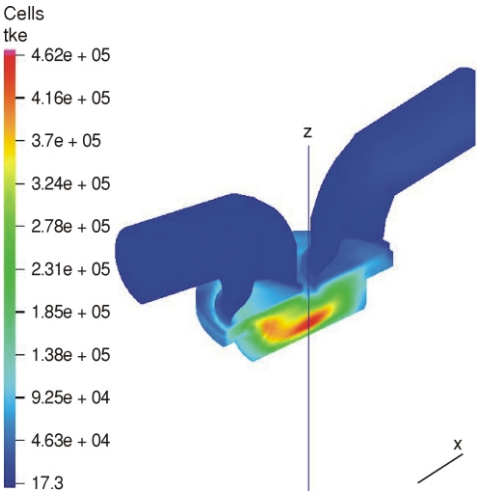

Figure 50. Spatial distribution of isocontours of kinetic energy of turbulence (tke) at 360 deg aTDC (SA = 54%), perspective plot (azimuth –130°, elevation +30°, twist 0°) (color image see on our web site)

perature in that point and time interval between the moment of flame arrival in that point and the moment when the temperature in that point reaches the value which is not sufficient to sustain the forward reaction (time of reaction or equilibrium delay). Obviously, NO concentration is a function of the change of spatial distribution of temperature in time. Spatial distribution of NO for different SA (44% and 54%) is shown in figs. 53-58.

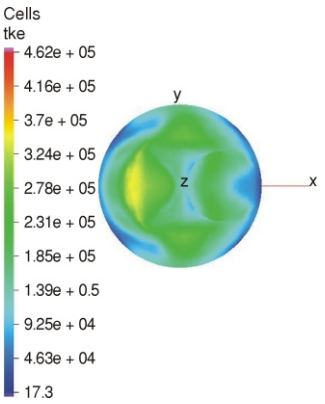

Figure 51. Spatial distribution of isocontours of kinetic energy of turbulence (tke) in x-y plane, z = 10.2 cm, at 360 deg aTDC (SA = 54%) (color image see on our web site)

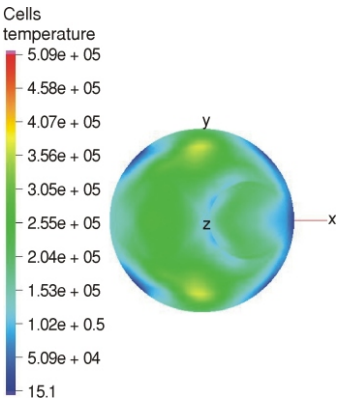

Figure 52. Spatial distribution of isocontours of kinetic energy of turbulence (tke) in x-y plane, z = 10.2 cm, at 360 deg aTDC (SA = 44%) (color image see on our web site)

The shape of iso contours of NO concentration pursues the shape of iso contours of temperature indicating that the commencement of NO formation coincides with flame arrival. It should be noted that the location of iso contours of maximum NO is

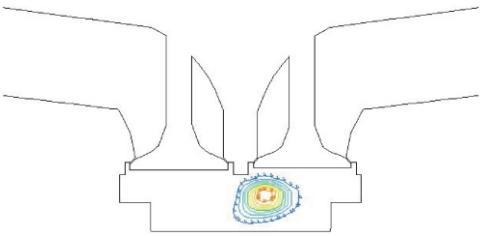

Figure 53. Spatial distribution of isocontours of NO concentration in x-z plane, y = 0.01 cm, at 345 deg aTDC (SA = 44%) (L = 9.589438 210^{-5}, H = 8.0304 10^{-4}) (color image see on our web site)

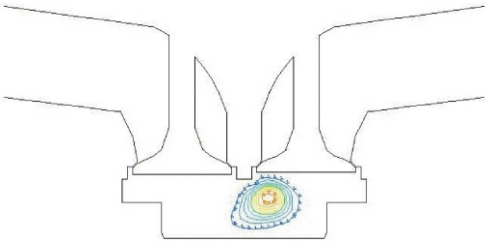

Figure 54. Spatial distribution of isocontours of NO concentration in x-z plane, y = 0.01 cm, at 345 deg aTDC (SA = 54%) (L = 1.032654 10^{-4}, H = 9.2934 10^{-4}) (color image see on our web site)

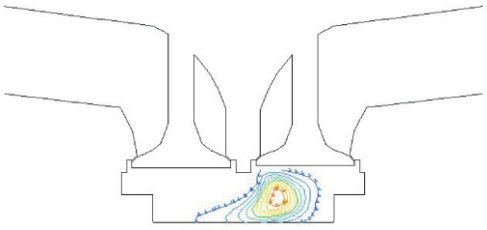

Figure 55. Spatial distribution of isocontours of NO concentration in x-z plane, y = 0.01 cm, at 360 deg aTDC (SA = 44%) (L = 8.24495 10^{-4}, H = 7.7206 10^{-3}) (color image see on our web site)

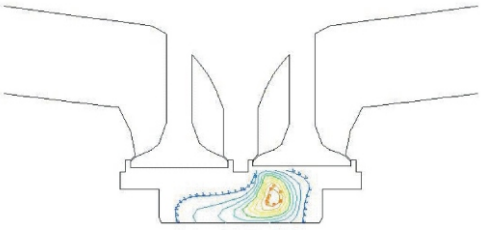

Figure 56. Spatial distribution of isocontours of NO concentration in x-z plane, y = 0.01 cm at 360 deg aTDC (SA = 54%) (L =1.012 10^{-3}, H = 9.116 10^{-3}) (color image see on our web site)

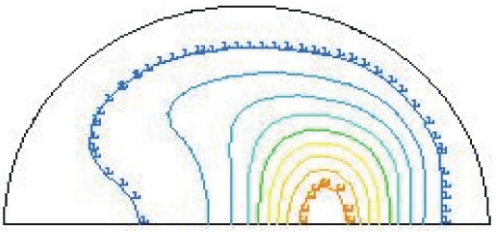

Figure 57. Spatial distribution of isocontours of NO concentration in x-y plane, z = 9.65 cm, at 360 deg aTDC (SA = 44%) (L = 6.9183 10^{-4}, H = 5.5027 10^{-3}) (color image see on our web site)

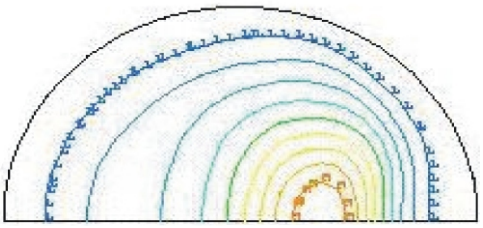

Figure 58. Spatial distribution of isocontours of NO concentration in x-y plane, z = 9.65 cm, at 360 deg aTDC (SA = 54%) (L = 8.6967 10^{-4}, H = 7.639 10^{-3}) (color image see on our web site)

in the zone of spark plug (shifted to the right) and follows the location of iso contours of maximum temperatures in all figures indicating that both the time of reaction (equilibrium delay) and spatial distribution of temperature are of critical importance for NO formation. Slightly higher temperature and faster flame propagation in the case of SA = 54% yield penalty as regards to NO. Namely the integral value of NO until 360 deg aTDC, in the case of SA = 54%, is $3.57243 \cdot 10^{-4}$ g while the corresponding integral value of NO, in the case of SA = 44%, is $2.833 \cdot 10^{-4}$ g.

Conclusions

In the case with no valves the squish plays an important role in flame front shape and its displacement. For particular combustion chamber with no valves three entirely different forms are encountered *i. e*. the insufficient squish (SA = 23-44%) yielding flame dominated flows, moderate squish (SA = 44-54%) yielding nearly spherical flame and excessive squish (SA = 63%) yielding squish dominated flame. For particular combustion chamber with valves the aforementioned flame characterizations are not valid at all *i. e*. flame front shape and its displacement are fully controlled by intake flow. The strong vortex flow around y-axis beneath the exhaust valve in the vicinity of TDC generated by intake flow annihilates entirely any effect of squish ranging from insufficient to excessive one and causes the detention of the flame propagation in that zone thereafter.

References

[1] Jovanović, Z., The Role of Tensor Calculus in Numerical Modeling of Combustion in I. C. Engines, in: Computer Simulation for Fluid Flow, Heat and Mass Transfer, and Combustion in Reciprocating Engines (Ed. N. Markator), Hemisphere Publishers, New York, USA, 1989, pp. 457-541
[2] Petrović, S., *et. al*., Modeling of Combustion in Otto-Cycle Engines (in Serbian), Faculty of Mechanical Engineering, University of Belgrade, Belgrade, 1995
[3] Jovanović, Z., Petrović, S., The Mutual Interaction between Squish and Swirl in S. I. Combustion Chamber, *Mobility and Vehicle Mechanics, 23* (1997), 3, pp. 72-86
[4] Chen, A., Lee, K. C., Yianneskis, M., Velocity Characteristics of Steady Flow through a Straight Generic Inlet Port, *International Journal for Numerical Methods in Fluids*, *21* (1995), 7, pp. 571-590
[5] Amsden, A. A., KIVA3V: A Block-Structured KIVA Program for Engines with Vertical or Canted Valves, Report LA-13313-MS, Los Alamos, N. Mex., USA, 1997
[6] AVL TYCON, Users Manual, version 4.3, 1998
[7] AVL BOOST, Users Manual, version 3.3, 2000

[8] Mahmood, Z., Chen, A., Yianneskis, M., On the Structure of Steady Flow through Dual Intake Engine Flow (internal report), Kings College, London, UK, 1999
[9] Jovanović, Z., Petrović, S., 3D Fluid Flow in I. C. Engine Combustion Chamber of Arbitrary Geometry, *Proceedings*, MOTOAUTO 97, Russe, Bulgaria, 1997, Vol. II, pp. 31-37
[10] Jovanović, Z., The Modification of the Combustion Chamber Geometry Layout on the Basis of Fluid Flow Pattern Criteria, *Proceedings*, MOTOAUTO 99, Plovdiv, Bulgaria, 1999, pp. 31-37
[11] Jovanović, Z., Petrović, S., The Effect of Squish Area Variation on Flame Front Shape and its Displacement, *Proceedings*, International Symposium Motor Vehicles – IC Engines, Kragujevac, Serbia, 1998, pp. 119-122
[12] Jovanović, Z., Petrović, S., Tomić, M., The New Fluid Flow Criterion for the Characterization of Flame Front Shape and its Displacement, *Proceedings*, VII International Scientific Conference Simulation Research in Automotive Engineering, Lublin, Poland, 1999, pp. 1-7
[13] Jovanović, Z., Petrović, S., The Effect of Tumble in Flame Front Shape and its Displacement in SI Engines, *Proceedings*, MOTOAUTO'03, Internal Combustion Engines, 2003, Sofia, Vol. I, pp.7-10
[14] Jovanović, Z., The Displacement of the Reverse Tumble Center of Rotation during Induction and Compression, *International Journal for Vehicle Mechanics, Engines and Transportation Systems, Mobility and Vehicle Mechanics*, *26* (2000), 1-2, pp. 29-44
[15] Jovanović, Z., The Mutual Interaction between Squish and Tumble in Combustion Chamber with Cylindrical Bowl, *Journal for Vehicle Mechanics, Engines and Transportation Systems, Mobility and Vehicle Mechanics*, *27* (2001), 1-2, pp. 19-32
[16] Jovanović, Z., Petrović, S., Basara, B., The Effect of Port De-Activation on Fluid Flow in Multi-Valve Engines, *Proceedings*, MOTOAUTO 2001, Varna, Bulgaria, pp. 47-52
[17] Jovanović, Z., Zeljković, I., The Modelling of Fluid Flow, Combustion and Emission in SI Engines – Multidimensional Approach (in Serbian), in: Equipment and Technologies for Emission Control from Stationary and Mobile Sources (Ed. M. Radovanović), Faculty of Mechanical Engineering, University of Belgrade, Belgrade, 1997, pp. 280-316
[18] Jovanović, Z., Petrović, S., Some Implications Concerning Macro Flows and Combustion in SI Engines, Mobility and Vehicle Mechanics, 2005, pp. 97-118
[19] CGS – Common Graphics System, LA Contract W-7405-ENG-36, Los Alamos, N. Mex., USA
[20] GMV – General Mesh Viewer, LA-UR-2986, Berkeley, Cal., USA

Authors´ addresses:

Z. S. Jovanović
Vinča Institute of Nuclear Sciences,
Center for Internal Combustion Engines and Motor Vehicles
P. O. Box 522, 11001 Belgrade, Serbia

S. V. Petrović, M. V. Tomić
University of Belgrade, Faculty of Mechanical Engineering,
Department for Internal Combustion Engines
16, Kraljice Marije, 11000 Belgrade, Serbia

Corresponding author Z. S. Jovanović
E-mail: zoranj@vin.bg.ac.yu

Paper submitted: October 19, 2007
Paper revised: November 30, 2007
Paper accepted: January 22, 2008